Stem Cell Research 53 (2021) 102352

Contents lists available at ScienceDirect

Stem Cell Research

journal homepage: www.elsevier.com/locate/scr

Edge-localized alteration in pluripotency state of mouse ES cells forming topography-confined layers on designed mesh substrates

Yuta Ando [a,b], Kennedy Omondi Okeyo [a,b,c,*], Junko Sunaga [b], Taiji Adachi [a,b,c]

[a] Department of Micro Engineering, Graduate School of Engineering, Kyoto University, Kyoto daigaku-katsura, Nishikyo-ku, Kyoto 615-8530, Japan
[b] Institute for Frontier Life and Medical Sciences, Kyoto University, 53 Shogoin Kawahara-cho, Sakyo-ku, Kyoto 606-8507, Japan
[c] Division of Systemic Life Science, Graduate School of Biostudies, Kyoto University, Yoshida-Konoecho, Sakyo-ku, Kyoto 606-8501, Japan

ARTICLE INFO

Keywords:
Embryonic stem cells
Pluripotency
Self-organization
Tissue topography
Cell adhesion
Mesh substrates

ABSTRACT

Self-organization of pluripotent stem cells during tissue formation is directed by the adhesion microenvironment, which defines the resulting tissue topography. Although the influence of tissue topography on pluripotency state has been inferred, this aspect of self-organization remains largely unexplored. In this study, to determine the effect of self-organized tissue topography on pluripotency loss, we designed novel island mesh substrates to confine the self-organization process of mouse embryonic stem cells, enabling us to generate isolated cell layers with an island-like topography and overhanging edges. Using immunofluorescence microscopy, we determined that cells at the tissue edge exhibited deformed nuclei associated with low OCT3/4, in contrast with cells nested in the tissue interior which had round-shaped nuclei and exhibited sustained OCT3/4 expression. Interestingly, F-actin and phospho-myosin light chain were visibly enriched at the tissue edge where ERK activation and elevated AP-2γ expression were also found to be localized, as determined using both immunofluorescence microscopy and RT-qPCR analysis. Since actomyosin contractility is known to cause ERK activation, these results suggest that mechanical condition at the tissue edge can contribute to loss of pluripotency leading to differentiation. Thus, our study draws attention to the influence of self-organized tissue topography in stem cell culture and differentiation.

1. Introduction

Multicellular tissue formation is driven by spatiotemporal cell dynamics including cell division, deformation, and rearrangement which collectively shape tissue topography depending on the adhesion microenvironment (Blanchard et al., 2009; Latorre et al., 2018). *In vitro* studies focusing on pluripotent stem cells (PSCs) have shown that self-organization is accompanied by the emergence of divergent cell populations with spatial variation in the levels of gene expression (Harrison et al., 2017; Takata et al., 2017). Indeed, the emergence of cell differentiation during self-organization of PSCs has been shown to be guided by biochemical and mechanical factors from the culture environment (Shahbazi et al., 2019; Takebe and Wells, 2019). In particular, the influence of mechanical factors on pluripotency and stem cell fate decision is a topic that has continued to attract a lot of attention, and has been investigated using 3D models formed by aggregation of PSCs (Warmflash et al., 2014; Shao et al., 2017). A recent study showed that colony-growing PSCs generate significant surface tension which was implicated in stem cell fate determination (Du et al., 2019). In addition, it has been suggested that the mechanical nature of PSCs at the colony edge may prime them for differentiation (Rosowski et al., 2015). These studies have highlighted how the interaction between PSCs and tissue topography leads to changes in their pluripotency state. However, precisely how self-organized tissue topography contributes to a change in pluripotency state remains largely unclear. Since self-organized tissue topography is a direct consequence of the cell adhesion, engineering the cell adhesion microenvironment is a viable approach to investigate differentiation and tissue formation in manner that recaptures key events of early embryonic development progresses (Xie et al., 2017; Sagy et al., 2019).

Previously, we have developed an *in vitro* culture platform employing microstructured mesh substrates to induce self-organization of cell sheets, relying solely on cell–cell contact (Okeyo et al., 2016). In the case of human induced pluripotent stem cells (hiPSCs), restricting cell-substrate adhesion using microfabricated mesh substrates has been shown to entice these cells to self-organize into 3D trophoblastic cysts

* Corresponding author at: Institute for Frontier Life and Medical Sciences, Kyoto University, 53 Shogoin Kawahara-cho, Sakyo-ku, Kyoto 606-8507, Japan
E-mail address: okeyo@infront.kyoto-u.ac.jp (K.O. Okeyo).

https://doi.org/10.1016/j.scr.2021.102352
Received 27 June 2020; Received in revised form 15 March 2021; Accepted 9 April 2021
Available online 15 April 2021

(Okeyo et al., 2015, 2018; Li et al., 2019). Furthermore, we have reported that mouse embryonic stem cells (mESCs) cultured on the mesh substrates can self-organize into cell layers and ultimately change their state into cells expressing primordial germ cell (PGC) markers (Ando et al., 2019). Although we succeeded in adjusting cell adhesion microenvironment to control self-organized layer formation using the mesh substrates, how tissue topography arising from self-organization may contribute to changes in pluripotency state remains to be clarified.

In the present study, we sought to investigate the influence of tissue topography on pluripotency state of self-organized stem cell layers formed on the microstructured mesh substrates. We noticed that mESCs cultured on the mesh substrates would self-organize into layers exhibiting topographically unique features defined by edge, trough and crest, with each of these zones showing distinct expression patterns. Therefore, we sought to further examine the contribution of tissue topography, and for this purpose, we designed a novel "island mesh" to induce self-organized formation of spatially isolated cell layers. Using this approach, we succeeded in generating distinctively demarcated island-like tissue topography with overhanging edges, which we then used to dissect the contribution of topography to pluripotency loss. We found that the overhanging edges, which were formed by cell layer protrusion in the absence of cell-substrate adhesion on the suspended island meshes, exhibited enriched F-actin bundles and underwent traceable retraction when ablated by laser, suggesting that they were under tension.

To discern the influence of edge-localized mechanical condition on pluripotency state of mESCs, we evaluated the expressions of OCT3/4 and AP-2γ; two markers which are known to show antagonistic expression pattern. Indeed, we found that, compared with cells in the tissue interior, edge cells exhibited low OCT3/4 expression and high AP-2γ expression, which correlated with pronounced phospho-myosin light chain (pMLC) expression and nuclear shape deformation, as confirmed by immunofluorescence microscopy. Furthermore, expresssion analysis of genes associated with the extracellular signal regulated kinase (ERK) focusing on cells with low OCT3/4 expression cells on the island mesh substrates suggested ERK activation. Interestingly, the distribution of phospho-ERK (pERK) as determined by immunofluorescence microscopy was consistent with the observed F-actin and pMLC enrichment at the tissue edges where OCT3/4 expression was predominantly low . Hence, we suggest the involvement of ERK signaling in the edge-localized change in the pluripotency state of mESCs on the topography-confining island mesh substates.

Taken together, these results suggest that tissue topography resulting from self-organization can in turn trigger pluripotency state transition in mESCs even under pluripotency maintenance culture conditions. Thus, this study highlights the influence of tissue topography on pluripotency state during stem cell self-organization, and draws attention to the importance of adjusting cell adhesion microenvironment in the induction of differentiation *in vitro*.

2. Materials and methods

2.1. Fabrication and setup of microstructured mesh substrates

Microstructured mesh substrates were fabricated by photolithography using SU-8 2 (MicroChem, USA), an epoxy-based negative photoresist, as reported previously (Ando et al., 2019). First, 2% gelatin from bovine skin (SAJ special grade; Sigma-Aldrich, USA) was spin-coated on a silicon wafer at 2,000 rpm. Gelatin coating formed a sacrificial layer for peeling-off the mesh substrates. Next, SU-8 2 was spin-coated at 2,000 rpm to form 2 μm-thick layer on a wafer, followed by baking at 65 °C for 1 min and 95 °C for 3 min. The wafer was then exposed to 10 mW/cm^2 ultraviolet light for 12 sec using a designed photomask, followed by post-baking at 65 °C for 1 min and 95 °C for 1 min. Pattern development was performed in propylene glycol methyl ether acetate (PGMEA), followed by rinsing in isopropanol. The exposed pattern was reinforced by laminating with a piece of Kapton polyimide film (Nitto, Japan) with a punched hole (4 mm in diameter), and then peeled off by immersion in a 50 °C water bath. Finally, the harvested mesh substrate was mounted on a 0.5 mm-thick silicon rubber spacer with a punched hole (6 mm in diameter). After fabrication, sterilization was performed under ultraviolet lump for at least 12 h.

2.2. Cell culture

mESCs were maintained in G-MEM (Wako, Japan) with 10% fatal bovine serum (FBS) (Sigma-Aldrich), 1 mmol/L sodium pyruvate (Wako), 1% MEM non-essential amino acids (Wako), 0.1 mmol/L 2-mercaptoethanol (Wako) and 1,000 units/mL leukemia inhibitory factor (LIF) (Wako). The cells were cultured at 37 °C and 5% CO_2 on cell culture dishes coated with 0.1% gelatin from porcine skin (gel strength 300, type A; Sigma-Aldrich). For passaging, cells were dissociated by TrypLE Express (Thermo Fisher Scientific, USA) and seeded at 7.0×10^3 cells/cm^2 for a 2-day culture duration or 2.6×10^3 cells/cm^2 for a 3-day culture duration.

2.3. Cell culture on microstrucrtured mesh substrates

mESCs on microstructured mesh substrates were cultured in the same culture medium as the pluripotency maintenance medium, but supplemented with antibiotic antimycotic (Sigma-Aldrich). For cell attachment on the mesh lines, protein coating was performed before cell seeding using 10 μg/mL laminin-511 E8 fragment (iMatrix-511 silk; Nippi, Japan) solution in phosphate buffered saline (PBS) for 12 h at 4 °C. Prior to seeding, the concentration of mESC suspension was adjusted to 1.0–5.0 $\times 10^6$ cells/mL, then a 100 μL of the cell suspension was gently added drop-by-drop onto the mesh substrates. Cells were then incubated for 6 h at 37 °C and 5% CO_2 to allow cell attachment on the mesh lines. To discard fallen cells, the mesh substrates seeded with cells were then transferred to a new culture dish and culture continued undisturbed in a fresh culture medium. In the case of inhibitor treatment, 10 μM of blebbistatin (Sigma-Aldrich) or 10 μM of Y-27632 (Wako) was added to the fresh culture medium at this stage. Day 0 was defined as the start of cell culture on the mesh substrates. In the case of continuous culture by Day 6, culture medium was exchanged at Day 3.

2.4. Cell lines and stable transfection

In this study, we used mESC lines E14tg2a (Riken Cell Bank, Japan) (Hooper et al., 1987) and OLV2-1 with knocked-in OCT3/4-linker-Venus vector (Riken Cell Bank) (Toyooka et al., 2008). The passage number of the E14tg2a and OLV2-1 cells used in this study was less than 20.

We also established E14tg2a cell line with knocked-in LifeAct-tdTomato. LifeAct-tdTomato plasmid vector expressed LifeAct (Riedl et al., 2008) tagged with tdTomato fluorescent protein on a pCAG promoter. The knock-in vector was amplified using standard bacterial transformation method of *E. coli* DH5α competent cells (Toyobo, Japan) with ampicillin. Then isolation of plasmid DNA was performed using QIAfilter Plasmid Midi and Maxi Kits (Qiagen, USA). To induce transfection in E14tg2a cells, cells seeded at 2.8×10^4 cells/cm^2 were cultured in the culture medium for 8 h, and then treated with 357 μL of 0.02 μg/μL plasmid in G-MEM containing 14 μL of FuGENE HD Transfection Reagent (Promega, USA) and further cultured for 40 h. To obtain cells expressing LifeAct-tdTomato, we expanded the transfected cells and then performed fluorescence activated cell sorting (FACS) by BD FACSMelody cell sorter (BD Biosciences, USA). After four rounds of passaging and cell sorting, we succeeded in establishing E14tg2a cell line stably expressing LifeAct-tdTomato. The passage number of the LifeAct-tdTomato knocked-in E14tg2a cells used in this study was less than 40.

2.5. Live cell imaging and multiphoton laser ablation

To capture the dynamics of Life-Act-tdTomato knocked-in cells on the mesh substrates, we performed timelapse microscopy at an interval of 2 h for 60 h using LCV-MPE multiphoton laser scanning incubator microscope (Olympus, Japan).

To confirm retraction of the tissue edge on the mesh substrates, multiphoton laser ablation was performed using FLUOVIEW FV1200MPE multi-photon laser scanning microscope (Olympus). Before laser ablation, timelapse images were acquired for 10 min. We incised a single point at the tissue edge using ultrafast Ti:Sappheire laser at 900 nm full power for 5–10 sec, followed by addtional timelapse imaging for 20 min to observe tissue deformation.

2.6. Cell staining and immunofluorescence microscopy

The cells were fixed with 4% paraformaldehyde in phosphate-buffered saline (PBS) for 30 min at room temperature, and then permeabilized with 0.1% polyethylene glycol mono-p-isooctylphenyl ether (Nacalai tesque, Japan) in PBS for 15 min at room temperature. After blocking with 3% bovine serum albumin (Sigma-Aldrich) in PBS for at least 30 min at room temperature, staining reagents diluted in 1% bovine serum albumin in PBS were added and incubated for 1 h at room temperature. For immunofluorescence staining, AP-2γ antibody (1:100; sc-12762; Santa Cruz Biotechnology, USA), NANOG antibody (1:200; ab80892; Abcam, UK), OCT3/4 antibody (1:100; sc-5279; Santa Cruz Biotechnology) and phospho-myosin light chain (pMLC) 2 (Thr18/Ser19) antibody (1:100; #3674; Cell Signaling Technology, USA), phospho-p44/42 MAPK (Erk1/2) (Thr202/Tyr204) antibody (1:200; #4370; Cell Signaling Technology) as primary antibody, and F(ab')2-goat anti-mouse IgG (H + L) cross-adsorbed secondary antibody Alexa Fluor 546 (1:500; A-11018; Thermo Fisher Scientific) and goat anti-rabbit IgG H&L Alexa Fluor 647 antibody (1:500; ab150079; Abcam) as secondary antibody were used. For staining cell nucleus and F-actin cytoskeleton, DAPI (1:500; D1306; Thermo Fisher Scientific) and Alexa Flour 647 phalloidin (1:100; A22287; Thermo Fisher Scientific) were used, respectively. Immunofluorescence microscopy was performed with FLUOVIEW FV3000 confocal laser scanning microscope (Olympus).

2.7. Image processing and quantitative analyses

Acquired immunofluorescence images were processed, reconstructed and visualized using ImageJ (National Institutes of Health, USA) and Imaris (Bitplane, Switzerland).

For quantitative analysis of cell nuclei, segmentation of cell nuclei was performed by "Segmentation Contour Mesh (B-HRBF)" function of VoTracer2 (http://www2.riken.jp/brict/Ijiri/VoTracer/index.html). After segmentation, intensity quantification of each cell nucleus was performed using 3D Roi Manager plugin (Ollion et al., 2013) in ImageJ. The mean intensities of OCT3/4-Venus and AP-2γ were normalized to mean intensities of DAPI and then the ratios of normalized intensities were calculated for each nucleus. In addition, ellipsoid fitting was performed using the same plugin above to analyze nuclei shape. The axes of the fitted ellipsoid were defined as major (L_1), second (L_2) and third axis (L_3), where $L_1 \geq L_2 \geq L_3$. Then elongation ratio was defined as L_1/L_2 and flatness ratio as L_2/L_3 for each nucleus.

Next, we analyzed quantitatively the distribution of F-actin, OCT3/4, AP-2γ, pMLC and pERK from the tissue edge (outer) toward the interior (inner) of the topographically confined cell layers on the island mesh substrates, based on confocal images sliced along the mesh plane. To generate an outline of a cell layer using ImageJ, automated thresholding was performed based on the F-actin or pERK images, followed by binarization, then smoothing by dilation and erosion. Each outline was further segmented into four concentric regions of interest, each 16-pixel in width from outer to inner. For each region of interest, the mean intensity values of each color channel were determined and then normalized to DAPI intensity. Finally, for presentation, the value for each region of interest was expressed as a ratio of the innermost region whose value was set at 1.

2.8. RNA isolation and RT-qPCR

Prior to RNA isolation, mesh-cultured cells were dissociated with TrypLE Express, followed by cell sorting using BD FACSMelody cell sorter. Manual gating based on forward and side scatter signals was performed to obtain a cell population. First, Venus-high gate was determined using OLV2-1 cells cultured on culture dish under pluripotency maintenance condition. Similarly, Venus-low gate was determined using unlabeled mESCs cultured on the island mesh substrates. For island mesh-cultured OLV2-1 cells, cell population with low OCT3/4-Venus expression was sorted based on the Venus-low gate. Visualization of the sorted cell population was performed using FlowJo single cell analysis software (BD Biosciences).

For real time quantitative polymerase chain reaction (RT-qPCR) analysis, we collected total RNA samples using ISOGEN II (Nippon Gene, Japan) and p-bromoanisole, and performed purification using NucleoSpin RNA (Macherey-Nagel, Germany), according to the manufacturer's instructions manuals. Preparation of total RNA samples was performed for both dish-cultured mESCs (N=6) and low OCT3/4-Venus expression OLV2-1 cells harvested from the island meshes (N=6). Reverse transcription reaction of isolated total RNA was performed using Transcriptor Universal cDNA Master (Sigma-Aldrich). RT-qPCR analysis was performed using StepOne Real-Time PCR System (Thermo Fisher Scientific) and PowerUp SYBR Green Master Mix (Thermo Fisher Scientific). The list of forward and reverse primers for RT-qPCR is shown in Supplementary Table 1. Relative levels of mRNA expression were assessed by the ΔΔCt method, with *Gapdh* as an internal control. All analyses were performed with three technical replicates. For the calculation of ΔCt, the outliers were statistically determined by the interquartile range (IQR) method with a decision range defined as three factors of IQR.

3. Results

3.1. Characterization of tissue topography arising from self-organization of mESCs on adhesion-limiting mesh substrates

Self-organization occurs under the influence of the cell adhesion microenvironment which dictates the underlying spatiotemporal events such as cell division, deformation, rearrangement, and differentiation (Miyoshi and Adachi, 2014; Kumar et al., 2017; Guilak et al., 2009; Kshitiz et al., 2012). Under our mesh culture platform employing highly porous mesh substrates to limit cell adhesion area, mESCs have been shown to self-organize through cell–cell contact to form cell layers (Ando et al., 2019). We therefore sought to examine how this self-organization on the mesh adhesion space shapes tissue topography, and the contribution of the resulting tissue topography to changes in pluripotency state. To this end, we performed detailed microscopic imaging of mESC undergoing proliferation and self-organization on the mesh substrates with large square mesh openings (>100 μm in size) and narrow mesh lines (5 μm in width) which were set suspended in a culture medium to restrict cell-substrate adhesion area (Fig. 1A). Cells were cultured on the mesh substrates using pluripotency maintaining medium with LIF-supplementation.

Despite the adhesion restriction, mESCs self-organized by cell–cell interaction to occupy the mesh openings, resulting in the formation of a cell layer exhibiting unique topographical features, namely "edges", "troughs" and "crests"; used in analogy of the wavy topography of the tissue surface, as depicted in Fig. 1B. Here, "edge" refers to the rim of the cell layer enclosing a partially filled mesh opening, "trough" to the depressions on the layer and "crest" to the thick zones of the layer

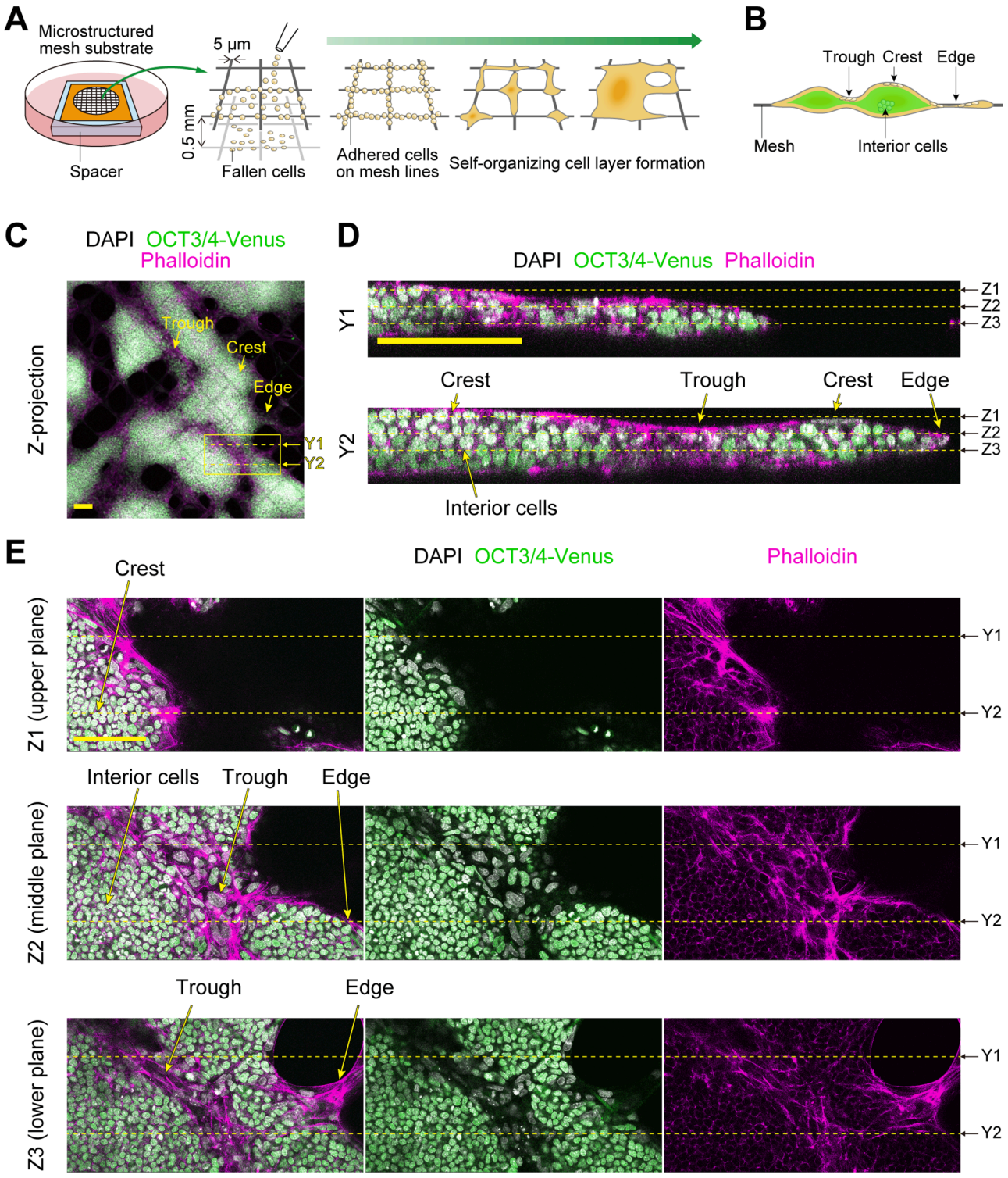

Fig. 1. Tissue topography of self-organized mESC layers on microstructured mesh substrates. (A) Schematic illustration of an island mesh substrate setup in a suspended position for cell seeding, and the self-organization processes leading to cell layer formation. (B) Schematic illustration of tissue topography formed on the mesh substrates. The resulting topographical features are indicated as "edge", "trough" and "crest". (C) Wide view of Z-projections of confocal images showing the topography of self-organized mESC layers on mesh substrates at Day 3. (D) Vertical (Y plane) cross-sections taken at positions (Y1, Y2 in E) of the cell layer region indicated by the yellow broken line in C. (E) Horizontal (Z plane) cross-sections at different heights (Z1, Z2, Z3 in D) of the cell layer region indicated by the yellow box in C. Topographical zones with well-established F-actin bundles were associated with low OCT3/4 expression. Scale bars: 100 μm. (For interpretation of the references to color in this figure legend, the reader is referred to the web version of this article.)

(Fig. 1C). It is worth noting that troughs appeared like zones of convergence which emerge when two edges around a crest advance toward one another and merge. Remarkably, a similar topography was confirmed using meshes of different mesh sizes. Notably, edges were more likely to form on large-size meshes, with a 200 μm mesh size yielding more edges than a 100 μm one (Supplementary Fig. 1). This confirms that the rate at which cells self-organize to fill-up an empty mesh, which is itself a factor of the mesh size, determines the emerging tissue topography. Since the two mesh sizes exhibited similar topographical features, we concluded that the resulting topographical features are not dependent on mesh size. Therefore, we settled on the 200 μm mesh size to further analyze the observed topographical features in relation to pluripotency state.

To clarify the effect of tissue topography on the pluripotency state of mESCs, we examined OCT3/4 expression (as a measure of pluripotency state) in comparison with F-actin development for each of the topographical features described above. Interestingly, 3D reconstruction of acquired confocal fluorescence images showed that whereas cells in the interior of a crest (interior cells) maintained OCT3/4 expression, peripheral cells on the tissue crest exhibited well-developed F-actin bundles but low OCT3/4 expression (Fig. 1D). Contrastingly, the tissue interior cells had relatively high OCT3/4 expression, round-shaped nuclei and poorly developed F-actin bundles compared with the peripheral cells. Contrastingly, troughs, which appeared like narrow trenches interspersing the crests, consisted of cells with low OCT3/4 expression but highly developed F-actin bundles (Fig. 1E). Similarly, tissue edges localized particularly at the borders of unfilled mesh openings also consisted of cells exhibiting reduced expression of OCT3/4 but highly developed F-actin bundles (Fig. 1E). A similar trend was observed for cell layers formed on 100 μm size mesh substrates and for cell layers maintained for an extended duration up to Day 6 (Supplementary Figs. 1 and 2).

Correctively, these results highlight that F-actin development correlates with low OCT3/4 expression in self-organized cell layers on the mesh substrates. Since F-actin development is a direct readout of a cell's mechanical environment (Heer and Martin, 2017), the above results also suggest that cells existing on the surface of crest, on the troughs and along the edges were under a mechanical condition different from the crest interior cells, and that this contributed to the change in pluripotency state. In other words, topography-associated F-actin bundle development and associated low OCT3/4 expression, particularly on the troughs and along the edges, suggests that pluripotency change may be mechanically triggered. We therefore sought to clarify this further by focusing on the tissue edges where probing the effects could be performed with relative ease, as detailed in the subsequent sections.

3.2. Self-organized formation of topography-confined cell layers with demarcated overhanging edges on a novel island mesh substrate

As mentioned above, low OCT3/4 expression colocalized with visibly pronounced F-actin development at the edges of the self-organized layers on the mesh substrates. Therefore, to probe the effect of tissue topography on the observed change in pluripotency state, we designed an original "island mesh substrate" to obtain self-organized cell layers with an island-like topography consisting of clearly demarcated overhanging edges.

The island mesh substrates consisted of isolated "square islands" of diagonal length 300 μm, with a separation distance of 600 μm in between two adjacent islands (Fig. 2A). Each island further consisted of finer 36 small square meshes with a diagonal length of 50 μm. The design was informed by our earlier observation that the rate of self-organization and mesh fill-up by mESCs could be modified by changing the size of mesh openings. mESC cultured on the island mesh substrates self-organized into isolated patches (islands) by Day 3 (Fig. 2B and C). Timelapse imaging was performed to capture the dynamics leading to the formation of island-like layers of mESCs on the substrates (Fig. 2D and Supplementary Movie 1). After seeding, cells proliferated and rapidly filled up the smaller 50 μm size mesh openings within one day after seeding. The resulting island-like layers grew thicker with time, and by Day 3, tissue edge could be seen protruding into the larger spaces surrounding the island, resulting in the formation of overhanging edges by Day 3 (Fig. 2D, arrows). Remarkably, the overhanging edges formed in the absence of cell-substrate adhesion, since the island meshes were set suspended in the culture medium. Hence, our novel island mesh enabled us to confine self-organization and generate an island-like topography consisting of a crest and distinctively demarcated overhanging edges.

We next examined the development of F-actin bundles at the overhanging edge using timelapse imaging of mESCs expressing LifeAct-tdTomato. The pluripotency state of these cells was confirmed by immunofluorescence microscopy (Supplementary Fig. 3A). As expected, F-actin intensity increased with increasing cell proliferation on the islands (Fig. 2D and Supplementary Movie 1). Given that overhanging edges were fully formed at Day 3, we chose this time point for further analysis of edge effect on pluripotency state of cells. First, we performed laser ablation using ultrafast laser in accordance with previous reports (Eiraku et al., 2011) to confirm edge retraction as a readout of mechanical tension. Here, the underlying assumption was that a material under circumferential tensile force would retract due to tension release when physically ablated with laser. To closely monitor the dynamics of the tissue rim during ablation analysis, we performed timelapse imaging for 10 min before and for 20 min after ablation (Fig. 2E and Supplementary Movie 2). Overhanging edges with clearly visible F-actin bundles were chosen for ablation, and laser was targeted very close to the extreme edge of tissue (Fig. 2E, yellow arrow heads). F-actin bundle at the targeted spot was incised, followed by retraction both in the circumferential and radial directions. Furthermore, using kymograph to track the dynamics of the retraction, we confirmed that edge retraction continued for about 10 min after ablation (Fig. 2E, bottom). Taken together, the laser ablation experiment provided qualitative evidence that the tissue edges of the island-like cell layers formed on the island meshes were under tension, as would be expected.

3.3. Edge-localized alteration in pluripotency state colocalized with F-actin and pMLC enrichment on island-like layers

Next, we sought to examine edge effect on topography-associated pluripotency alteration as evidenced by edge-localized low OCT3/4 expression in Fig. 1. To this end, we compared the expressions of OCT3/4 and AP-2γ relative to the topography of the self-organized layers on the island mesh substrates at Day 3. These two markers were chosen based on our previous study which had confirmed the expression of PGC-like genes in self-organized mESC layers on the mesh substrates (Ando et al., 2019). AP-2γ has been associated with early embryonic differentiation, such as in PGC or trophoblast differentiation (Hayashi et al., 2011; Adachi et al., 2013). For the purposes of verification, AP-2γ expression was determined and found to be relatively low in mESCs cultured under pluripotency maintenance condition on a typical culture dish (Supplementary Fig. 3B). Edge effect on OCT3/4 and AP-2γ expressions was examined by confocal immunofluorescence microscopy. 3D reconstruction of the confocal images confirmed an island-like topography with overhanging edges (Fig. 3A, upper left). Consistent with the results of Fig. 1, edge-localized cells showed weak expression of OCT3/4 but relatively strong expression of AP-2γ (Fig. 3A, right). In contrast, the interior cells exhibited relatively high OCT3/4 but low AP-2γ expressions (Fig. 3A, lower left). As revealed by phalloidin staining, F-actin was highly enriched at the tissue edges with clearly visible bundles compared with interior cells (Fig. 3A, right). Indeed, the interior cells exhibited actin cortex directly underneath the plasma membrane but lacked visible F-actin bundles.

Remarkably, we noticed that AP-2γ expression was particularly strong in cells with elongated nuclear morphology at the tissue edges

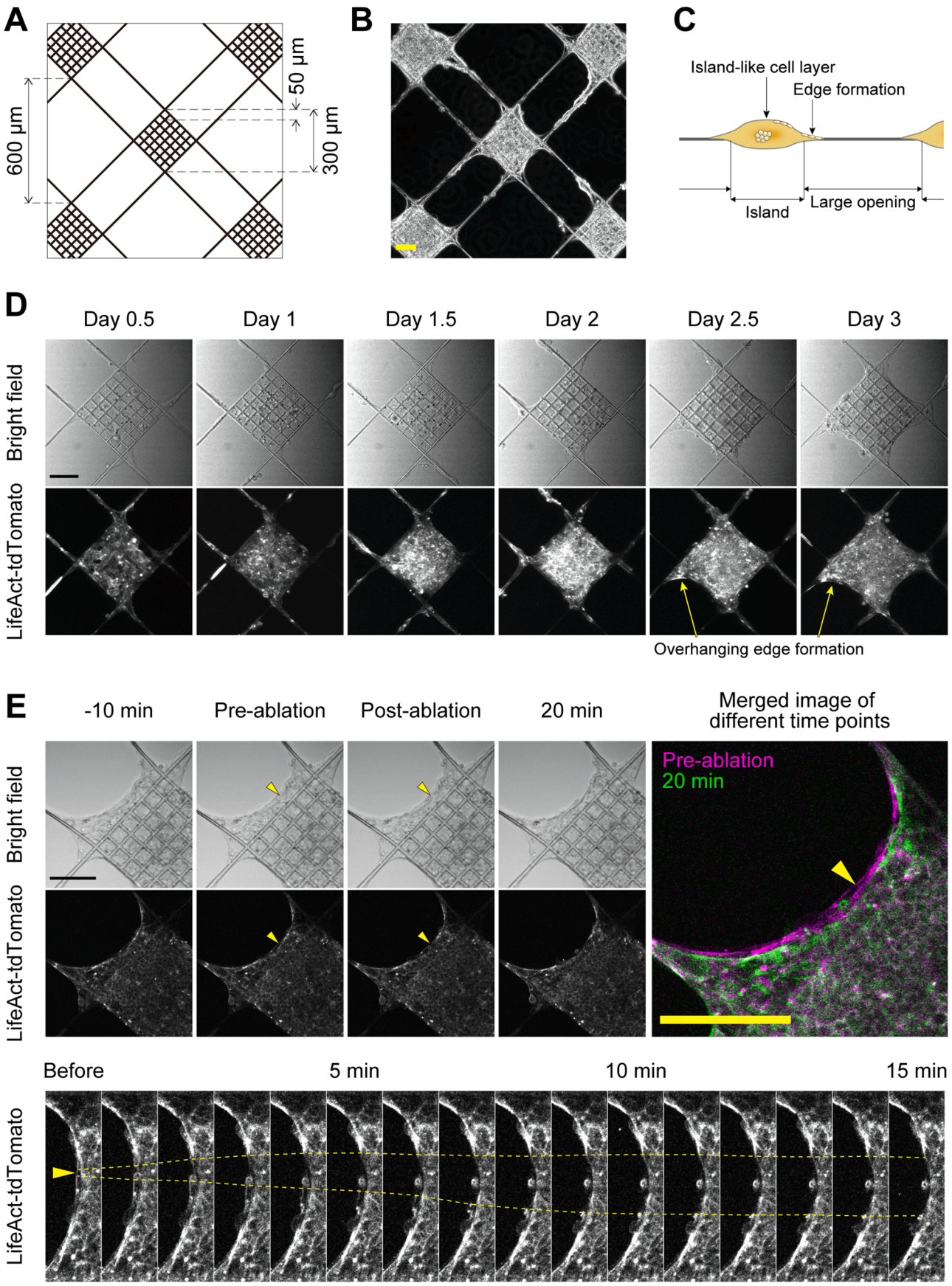

(caption on next page)

Fig. 2. Island mesh substrates designed to induce self-organization of topography-confined island-like layers with overhanging edges. (A) A schematic of an island mesh substrate showing spatially separated "islands" each consisting of 36 small square meshes with a diagonal length of 50 μm. The separation distance between adjacent islands was 600 μm. (B) A microscopic image showing isolated cell layers formed on an island mesh substrate at Day 3. (C) A schematic illustration of tissue topography formed on an island mesh substrate. (D) Timelapse images showing self-organized formation of an island-like cell layer by mESCs expressing LifeAct-tdTomato. Overhanging edges were formed by cell layer outgrowth by Day 3. (E) Representative timelapse images showing edge retraction following laser ablation. The yellow arrowhead indicates the ablated spot at the outermost edge. A pseudo-colored composite image depicting the position of edge before and after retraction. The image was created by overlaying pseudo-colored images at 10 min pre-ablation and 20 min post-ablation. Kymograph representation of retraction dynamics following incision of F-actin bundle at the ablated spot. Retraction occurred both in the circumferential and radial directions for a period of 10 min after ablation. Scale bars: 100 μm. (For interpretation of the references to color in this figure legend, the reader is referred to the web version of this article.)

(Fig. 3B, upper). Since nuclear shape is a readout of the cell's mechanical condition, we statistically compared nuclear morphology between peripheral cells and interior cells. Using ellipsoid fitting, we confirmed quantitatively that peripheral cells had highly deformed nuclei (elongated and/or flattened), as shown by the results (Fig. 3B, lower). Notably, cells with round-shaped nuclei (low elongation and flatness ratios) exhibited relatively high OCT3/4 expression. On the other hand, cells with elongated or flattened nuclei tended to have relatively high AP-2γ expression. This suggests a correlation between nuclear deformation and pluripotency state change at the periphery. To further confirm the mechanical condition at the overhanging edge, we next performed immunofluorescence microscopy of pMLC, which interact with F-actin bundles to generate contractile force in nonmuscle cells. pMLC was visibly pronounced at the tissue edge, consistent with F-actin distribution (Fig. 3C), Considering the observed edge retraction upon ablation, this suggests the presence of mechanical tension at the overhanging edges of the island-like cell layers.

Next, we quantified the distribution of OCT3/4, AP-2γ, F-actin and pMLC expression from the tissue edge toward the interior, based on the captured immunofluorescence images (Supplementary Fig. 4A). The results clearly showed high intensities of F-actin and pMLC at the tissue edge (outer), with a drastic decline in intensity toward the interior (inner), implying the edge-localization (Fig. 3D). Similarly, AP-2γ was strongly expressed in the outer region compared with the inner region (Fig. 3D). OCT3/4 expression did not exhibit a clear tendency mainly because some cells at the outermost edge still expressed OCT3/4. Taken together, these results suggest that edge-localized mechanical condition may have contributed to alteration in pluripotency state. To further confirm this, we treated the cell layers on the island mesh with blebbistatin, a nonmuscle myosin II inhibitor, or Y-27632, a Rho-associated protein kinase inhibitor, both of which repress tension generation via inhibition of actomyosin contraction. However, compared with untreated samples, we did not observe any clear differences for the concentrations used (Supplementary Fig. 4B and C).

In summary, we have demonstrated that elevated AP-2γ expression and low OCT3/4 expression correlates well with F-actin and pMLC enrichment at the tissue edge, which suggests the involvement of edge-localized mechanical tension. Moreover, similar observations were also made for the topography-confined cell layers at Day 6 (Supplementary Fig. 5). Considering that mESCs usually maintain their pluripotency for about 3 days under the standard maintenance culture, these observations highlight that tissue topography arising from self-organization on the mesh platform can create a mechanical condition which in turn may trigger a change in pluripotency state.

3.4. Pluripotency state alteration on the island mesh substrates is associated with ERK activation at the tissue edge

A key finding of this study was that, compared with cells residing in the tissue interior, cells located at the tissue edge exhibited F-actin and pMLC enrichment, comparatively low OCT3/4 expression, and high AP-2γ expression (Fig. 3). To gain a mechanistic perspective on the influence of topography on the pluripotency change, we conducted further gene and protein expression analyses focusing on the tissue edge. For gene expression analysis, first we sorted mESCs with low OCT3/4-Venus expression (presumed to be edge-localized cells) harvested from the island meshes at Day 3 (Fig. 4A and Supplementary Fig. 6). Then, we performed RT-qPCR analysis for this cell population, and compared their mRNA expression level with those of control dish-cultured mESCs at Day 3 (Fig. 4B). While *Pou5f1* (encoding OCT3/4) expression was similar, *Nanog* expression level was comparatively higher in cells with low OCT3/4-Venus expression than in control cells. *Tfap2c* (encoding AP-2γ) and *Prdm1* (encoding BLIMP1) expressions were elevated in low OCT3/4-Venus cells. Remarkably, elevated *Tfap2c* expression was consistent with the results of immunofluorescence microscopy.

In addition, expression analysis was performed for genes associated with ERK activation, including *Myc*, *Map2k1* (encoding MEK1), *Mapk3* (encoding ERK1) and *Dusp6* (Fig. 4B). *Myc*, an important gene for maintaining self-renewal and pluripotency (Smith et al., 2010), was comparatively weakly expressed in the low OCT3/4-Venus cells than in control. Moreover, the expression of *Map2k1* and *Mapk3* was elevated in low OCT3/4-Venus population, consistent with *Myc* suppression of ERK signaling to prevent differentiation (Hishida et al., 2011). Contrastingly, the expression of *Dusp6*, a phospho-ERK1/2 phosphatases (Yang et al., 2012), was slightly lower in low OCT3/4-Venus cells, which hinted to ERK activation.

To confirm ERK activation at the tissue edge, we performed immunofluorescence confocal microscopy with focus on pERK expression (Fig. 4C). Intriguingly, pERK expression was pronounced at the tissue edge with dominantly low OCT3/4 expression (Fig. 4C). AP-2γ expression was also pronounced at the tissue edge, consistent with the results in Fig. 3. Quantification of the distribution of these markers from the edge toward the tissue interior clearly demonstrated higher expression of pERK and AP-2γ at the edge compared with the interior (Fig. 4D). Interestingly, treatment with Y-27632 to modulate actomyosin contraction showed a slight reduction in pERK expression at the edge, although this result was not statistically significant (Supplementary Fig. 7). Collectively, these results suggest that ERK activation might play a role in pluripotency state alteration leading to the observed low OCT3/4 expression at the edge of self-organized tissues on the island mesh substrates.

4. Discussion

In this study, we hypothesized that tissue topography arising from self-organization under the instruction of adhesion environment can in turn influence pluripotency state. To explore this, we designed the island mesh substrates to induce the formation of topographically isolated cell layers, enabling us to associate tissue edge with alteration in pluripotency state during self-organization of mESCs. We have demonstrated edge-localized F-actin and pMLC enrichment associated with low OCT3/4 and high AP-2γ expressions (Fig. 3). Importantly, we have showed that cells at tissue edges equally exhibited high expression of pERK (Fig. 4), which spatially correlated well with F-actin bundles and pMLC (Fig. 3). These results suggest the involvement of edge-localized mechanical condition in the loss of pluripotency, as evidenced by low OCT3/4 expression.

The fact that change in pluripotency state begins at the edge as early as Day 3 in self-organized cell layers of mESCs under LIF-supplemented culture condition, and in a topography-triggered manner is biologically exciting. Previous studies have shown that tissue topography emerging from self-organization under mechanical constraint is an important

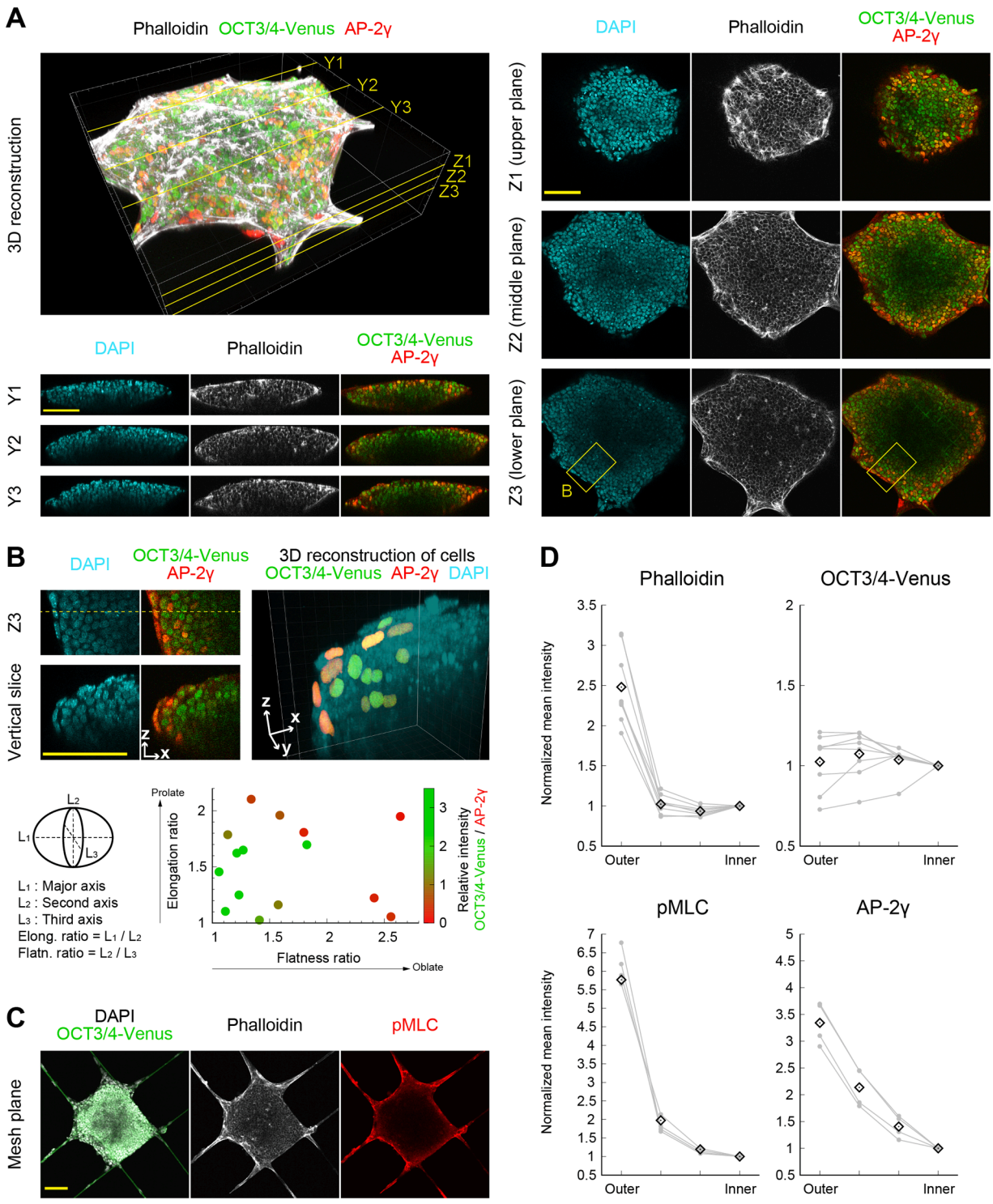

Fig. 3. Edge-localized alteration in pluripotency state of self-organized mESC layer on an island mesh substrate at Day 3. (A) *Upper left*: A 3D reconstructed image of an island-like mESC layer formed on an island mesh. *Lower left*: Vertical (Y plane) cross-section images along the lines indicated by Y1, Y2, and Y3 in the 3D reconstructed image. *Right*: Horizontal (Z place) cross-section images along the heights indicated by Z1, Z2, and Z3 in the 3D reconstructed image. The cross-sections show peripheral cells (edge cells) with highly reduced OCT3/4 expression compared with interior cells which exhibit sustained expression. F-actin enrichment and relatively high AP-2γ expression at the tissue periphery (edges) is also apparent. (B) *Upper left*: Enlarged view of the boxed region in A-Z3 depicting nuclear deformation at the tissue edge. *Upper right*: 3D reconstruction of sliced images taken from the boxed region in A-Z3. *Lower*: Result of quantification of nuclear shape of edge cells by ellipsoid fitting. Cells with highly deformed nuclei (prolate or oblate spherical shapes) at the tissue edge showed relatively higher AP-2γ expression. In contrast, cells with round-shaped nuclei were mostly in the tissue interior and exhibited relatively higher OCT3/4 expression. (C) Horizontal cross-section images taken at the mesh substrate plane depicting high expression of F-actin and pMLC at the tissue edge. (D) Intensity analysis from the edge toward to the tissue interior for the indicated proteins. Mean intensity of each region of interest was normalized with that of the innermost region. Gray lines indicate the normalized mean values for individual samples quantified, while black diamond marks indicate the mean values of all samples for each region of interest. The number of analyzed samples were N=8 for phalloidin and OCT3/4-Venus, and N=4 for pMLC and AP-2γ, respectively. Scale bars: 100 μm.

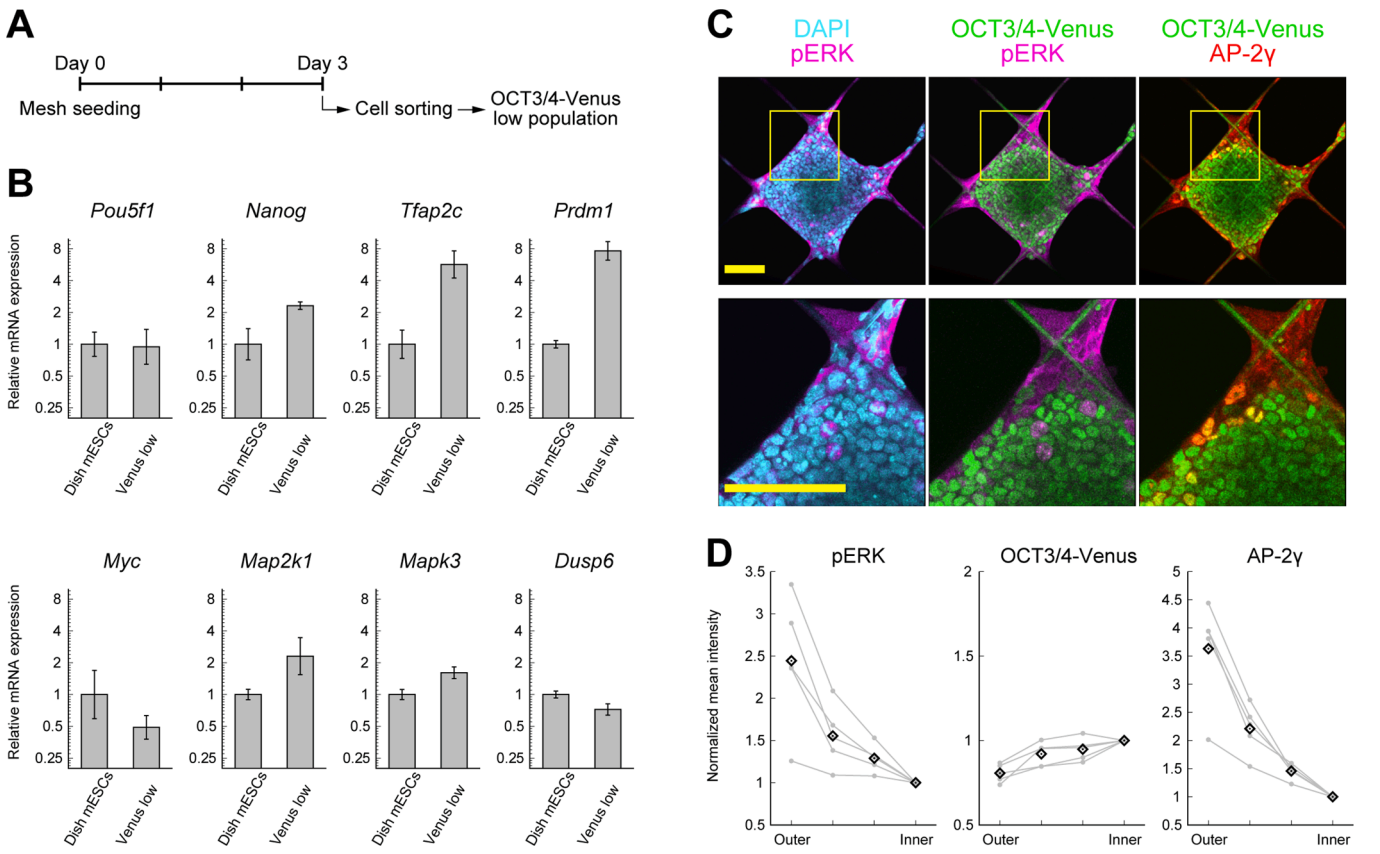

Fig. 4. Edge-localized ERK activation associated with pluripotency alteration at the tissue edge. (A) A workflow for RT-qPCR analysis from cell seeding to cell sorting. Low OCT3/4-Venus expression cells were obtained by cell sorting at Day 3. (B) RT-qPCR analysis at Day 3 for mRNA expression of pluripotency markers (*Pou5f1* and *Nanog*), germ cell markers (*Tfap2c* and *Prdm1*) and ERK-related genes (*Myc*, *Map2k1*, *Mapk3* and *Dusp6*). Individual mRNA expression was normalized against *Gapdh* and relative values were presented in log2 scale, with standard deviations. (C) Characterization of pERK expression using immunofluorescence confocal microscopy. *Upper*: Horizontal cross-sections along the mesh substrate plane. *Lower*: High magnification images of the boxed region in the upper images. Pronounced pERK expression was localized at the tissue edge and correlated well with low OCT3/4 expression. Scale bars: 100 μm. (D) Intensity analysis of pERK distribution from the edge toward to the tissue interior in comparison with OCT3/4 and AP-2γ. The number of analyzed samples were N=5. The intensity analysis and notations used are as indicated in Fig. 3D.

factor in multicellular tissue morphogenesis (Karzbrun et al., 2018; Desmaison et al., 2018). In fact, attempts have been made to constrain shape of stem cell tissues to elucidate effects on cell differentiation (Hiramatsu et al., 2013; Matsushiro et al., 2018). We have succeeded in generating topography-confined stem cell tissues with clearly demarcated edges using designed island mesh substrates, permitting us to probe the influence of self-organized tissue topography on pluripotency. F-actin and pMLC enrichment at the tissue edge, where protrusion occurs without substrate support, can be regarded as a direct consequence of tension, which is required for their stabilization (Heer and Martin, 2017). Although mechanical tension was not fully quantified in our study, the laser ablation results (Fig. 2E), together with the observed nuclear deformation (Fig. 3B), qualitatively suggested the presence of edge-localized mechanical tension, whose contribution to the observed low OCT3/4 and high AP-2γ expression at the tissue edge was explored. Indeed, past studies have associated increased F-actin formation with PSC differentiation (Li et al., 2017; David et al., 2019).

Previous studies have shown that ERK signaling plays an integral role in pluripotency alteration and is highly involved in the response to mechanical tension (Verstreken et al., 2019). Based on the finding that ERK activation was localized at the tissue edge (Fig. 4), we postulated that edge-localized mechanical tension may trigger alteration in pluripotency state, possibly via ERK signaling pathway even under LIF-dependent culture condition on the mesh substrates. Indeed, ERK signaling is known to be affected by actomyosin contractility (Hirata and Sokabe, 2015), and has been reported to regulate protrusion during cell migration via F-actin polymerization (Mendoza et al., 2015). Thus, we argue that down-regulation of OCT3/4 and, contrastingly, up-regulation of germ cell markers such as AP-2γ may have been triggered by edge-localized mechanical condition, possibly via ERK activation at the tissue edge (Fig. 5). AP-2γ is a core factor in the PGC transcription network and is known to be essential for PGC differentiation (Hayashi et al., 2011; Kimura et al., 2014). In our previous study, we reported up-regulation of AP-2γ in self-organized mESCs on mesh substrates, which we associated with PGC-like differentiation (Ando et al., 2019). Moreover, AP-2γ has been reported to suppress OCT3/4 expression during forced induction of trophoblastic differentiation, and to act cooperatively with SOX2 in trophoblast stem cells (Adachi et al., 2013). Indeed, it has been showed that PGC-related genes in mESCs are affected by the MYC/MAX complex, which suppresses ERK signaling to prevent differentiation (Hishida et al., 2011; Maeda et al., 2013). RT-qPCR results (Fig. 4B) showed a reduced expression of *Myc*, which also implies ERK activation to support differentiation.

Although our study suggests that alteration in pluripotency state can be affected by tissue topography via ERK activation, a major limitation of our study is that we could not establish a detailed mechanoregulatory pathway for the involvement of mechanical tension in ERK activation. Specifically, the results of inhibition experiments to modulate actomyosin tension showed only a slight reduction in F-actin, pMLC and pERK expressions and were not conclusive, partly because only partial inhibition could be achieved at the inhibitor concentrations used in our study. Higher concentration severely affected tissue formation on the

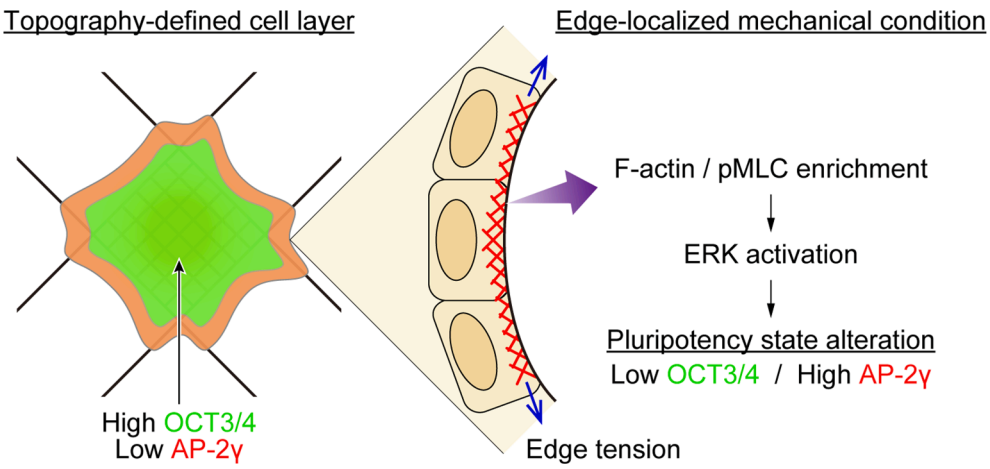

Fig. 5. A schematic showing association between tissue topography and pluripotency state alteration in self-organized cell layer on an island mesh substrate. Edge formation without substrate support on the suspended island mesh substrate is expected to require enhanced F-actin and pMLC development at the tissue edge, as observed in this study. In turn, the resulting actomyosin contractility (edge tension) might activate ERK-associated signaling pathway, leading to the observed pluripotency state alteration at the tissue edge.

island mesh substrates. Thus, we could not rule out the possibility of ERK activation via other factors. For instance, a reduction in membrane tension has been shown to induce ERK activation via endocytosis of fibroblast growth factor (FGF) signaling components, leading to the exit from pluripotency state (Belly et al., 2021).

Collectively, our results shed light on how self-organized topography formation may create a local mechanical condition which triggers spatial alteration in pluripotency state in an outside-inside manner. Future works will explore mechanosensitive pathways via which tissue topography may facilitate the onset of fate determination during PSC self-organized tissue formation.

5. Conclusion

In this study, we investigated changes in pluripotency state in relation to self-organized tissue topography resulting from collective cellular dynamics on adhesion-limiting microstructured mesh substrates under pluripotency maintenance culture condition. For this purpose, we designed a novel island mesh substrate which could trigger self-organization in an isolated fashion, enabling us to generate topography-confined mESC layer for probing the association between tissue topography and alteration in pluripotency state. Our results show that cells at the tissue edge exhibited F-actin and pMLC enrichment as well as nuclear deformation, which can be considered as a manifestation of the underlying mechanical condition. Moreover, we further confirmed that compared with interior cells, edge-localized cells showed low OCT3/4 and contrastingly high AP-2γ expressions. Furthermore, the results of RT-qPCR analysis and immunofluorescence characterization suggested ERK activation at the tissue edge where cells with low OCT3/4 expression were predominantly located. Since actomyosin contractility has been implicated in ERK activation, these results highlight that mechanical condition created by self-organized topography formation can contribute to alteration in pluripotency state, particularly at the tissue edge. Thus, controlling tissue topography by engineering the cell adhesion microenvironment is a viable approach to modulate stem cell fate decision making *in vitro*.

CRediT authorship contribution statement

Yuta Ando: Investigation, Methodology, Writing - original draft, Visualization. **Kennedy Omondi Okeyo:** Conceptualization, Methodology, Writing - review & editing, Resources, Funding acquisition. **Junko Sunaga:** Investigation, Resources. **Taiji Adachi:** Writing - review & editing, Resources, Supervision, Funding acquisition.

Declaration of Competing Interest

The authors declare that they have no known competing financial interests or personal relationships that could have appeared to influence the work reported in this paper.

Acknowledgements

This research was supported by AMED under Grant Numbers JP19gm5810023 and JP20gm5810023, and JSPS KAKENHI Grant Number JP16H06486. Support for the publication of this article was provided by the Future Development Funding Program of Kyoto University Research Coordination Alliance. We are grateful to Naotaka Nakazawa and Mineko Kengaku (Institute for Integrated Cell-Material Sciences, Kyoto University, Japan) for gifting us with LifeAct-tdTomato plasmid vector and for giving us technical advice. We are thankful to lab members Koichiro Maki and Yoshikiyo Kibe for help with experiments and useful discussion. We are grateful to the staff of Kyoto University Nano Technology Hub in "Nanotechnology Platform Project" for technical support with the fabrication of mesh substrates used in this study.

Appendix A. Supplementary data

Supplementary data to this article can be found online at https://doi.org/10.1016/j.scr.2021.102352.

References

Adachi, K., Nikaido, I., Ohta, H., Ohtsuka, S., Ura, H., Kadota, M., Wakayama, T., Ueda, H.R., Niwa, H., 2013. Context-dependent wiring of Sox2 regulatory networks for self-renewal of embryonic and trophoblast stem cells. Mol. Cell 52, 380–392.

Ando, Y., Okeyo, K.O., Adachi, T., 2019. Modulation of adhesion microenvironment using mesh substrates triggers selforganization and primordial germ cell-like differentiation in mouse ES cells. APL Bioeng. 3, 016102.

Belly, H.D., Stubb, A., Yanagida, A., Labouesse, C., Jones, P.H., Paluch, E.K., Chalut, K.J., 2021. Membrane tension gates ERK-mediated regulation of pluripotent cell fate. Cell Stem Cell 28, 273–284.

Blanchard, G.B., Kabla, A.J., Schultz, N.L., Butler, L.C., Sanson, B., Gorfinkiel, N., Mahadevan, L., Adams, R.J., 2009. Tissue tectonics: morphogenetic strain rates, cell shape change and intercalation. Nat. Methods 6, 458–464.

David, B.G., Fujita, H., Yasuda, K., Okamoto, K., Panina, Y., Ichinose, J., Sato, O., Horie, M., Ichimura, T., Okada, Y., Watanabe, T.M., 2019. Linking substrate and nucleus via actin cytoskeleton in pluripotency maintenance of mouse embryonic stem cells. Stem Cell Res. 41, 101614.

Desmaison, A., Guillaume, L., Triclin, S., Weiss, P., Ducommun, B., Lobjois, V., 2018. Impact of physical confinement on nuclei geometry and cell division dynamics in 3D spheroids. Sci. Rep. 8, 8785.

Du, J., Fan, Y., Guo, Z., Wang, Y., Zheng, X., Huang, C., Liang, B., Gao, L., Cao, Y., Chen, Y., Zhang, X., Li, L., Xu, L., Wu, C., Weitz, D.A., Feng, X., 2019. Compression generated by a 3D supracellular actomyosin cortex promotes embryonic stem cell colony growth and expression of Nanog and Oct4. Cell Syst. 9, 214–220.

Eiraku, M., Takata, N., Ishibashi, H., Kawada, M., Sakakura, E., Okuda, S., Sekiguchi, K., Adachi, T., Sasai, Y., 2011. Self-organizing optic-cupmorphogenesis in three-dimensional culture. Nature 472, 51–56.
Guilak, F., Cohen, D.M., Estes, B.T., Gimble, J.M., Liedtke, W., Chen, C.S., 2009. Control of stem cell fate by physical interactions with the extracellular matrix. Cell Stem Cell 5, 17–26.
Harrison, S.E., Sozen, B., Christodoulou, N., Kyprianou, C., Zernicka-Goetz, M., 2017. Assembly of embryonic and extraembryonic stem cells to mimic embryogenesis in vitro. Science 356, eaal1810.
Hayashi, K., Ohta, H., Kurimoto, K., Aramaki, S., Saitou, M., 2011. Reconstitution of the mouse germ cell specification pathway in culture by pluripotent stem cells. Cell 146, 519–532.
Heer, N.C., Martin, A.C., 2017. Tension, contraction and tissue morphogenesis. Development 144, 4249–4260.
Hiramatsu, R., Matsuoka, T., Kimura-Yoshida, C., Han, S., Mochida, K., Adachi, T., Takayama, S., Matsuo, I., 2013. External mechanical cues trigger the establishment of the anterior-posterior axis in early mouse embryos. Dev. Cell 27, 131–144.
Hirata, H., Sokabe, M., 2015. A novel role of actomyosin in ERK singaling. Commun. Integr. Biol. 8, e1017176.
Hishida, T., Nozaki, Y., Nakachi, Y., Mizuno, Y., Okazaki, Y., Ema, M., Takahashi, S., Nishimoto, M., Okuda, A., 2011. Indefinite self-renewal of ESCs through Myc/Max transcriptional complex-independent mechanisms. Cell Stem Cell 9, 37–49.
Hooper, M., Hardy, K., Handyside, A., Hunter, S., Monk, M., 1987. HPRT-deficient (Lesch-Nyhan) mouse embryos derived from germline colonization by cultured cells. Nature 326, 292–295.
Karzbrun, E., Kshirsagar, A., Cohen, S.R., Hanna, J.H., Reiner, O., 2018. Human brain organoids on a chip reveal the physics of folding. Nat. Phys. 14, 515–522.
Kimura, T., Kaga, Y., Ohta, H., Odamoto, M., Sekita, Y., Li, K., Yamano, N., Fujikawa, K., Isotani, A., Sasaki, N., Toyoda, M., Hayashi, K., Okabe, M., Shinohara, T., Saitou, M., Nakano, T., 2014. Induction of primordial germ cell-like cells from mouse embryonic stem cells by ERK signal inhibition. Stem Cells 32, 2668–2678.
Kshitiz, Park, J., Kim, P., Helen, W., Engler, A.J., Levchenko, A., Kim, D-H., 2012. Control of stem cell fate and function by engineering physical microenvironment. Integr. Biol. 4, 1008–1018.
Kumar, A., Placone, J.K., Engler, A.J., 2017. Understanding the extracellular forces that determine cell fate and maintenance. Development 144, 4261–4270.
Latorre, E., Kale, S., Casares, L., Gómez-González, M., Uroz, M., Valon, L., Nair, R.V., Garreta, E., Montserrat, N., Del Campo, A., Ladoux, B., Arroyo, M., Trepat, X., 2018. Active superelasticity in three-dimensional epithelia of controlled shape. Nature 563, 203–208.
Li, J., Minami, I., Shiozaki, M., Yu, L., Yajima, S., Miyagawa, S., Shiba, Y., Morone, N., Fukushima, S., Yoshida, M., Li, S., Qiao, L., Li, X., Wang, L., Kotera, H., Nakatsuji, N., Sawa, Y., Chen, Y., Liu, L., 2017. Human pluripotent stem cell-derived cardiac tissue-like constructs for repairing the infarcted myocardium. Stem Cell Rep. 9, 1546–1559.
Li, Z., Kurosawa, O., Iwata, H., 2019. Establishment of human trophoblast stem cells from human induced pluripotent stem cell-derived cystic cells under micromesh culture. Stem Cell Res. Therapy 10, 245.
Maeda, I., Okamura, D., Tokitake, Y., Ikeda, M., Kawaguchi, H., Mise, N., Abe, K., Noce, T., Okuda, A., Matsui, Y., 2013. Max is a repressor of germ cell-related gene expression in mouse embryonic stem cells. Nat. Commun. 4, 1754.
Matsushiro, Y., Kato-Negeshi, M., Onoe, H., 2018. Differentiation of 3D-shape-controlled mouse neural stem cell to neural tissues in closed agarose microchambers. Biotech. Bioeng. 115, 1614–1623.
Mendoza, M.C., Vilela, M., Juarez, J.E., Blenis, J., Danuser, G., 2015. ERK reinforces actin polymerization to power persistent edge protrusion during motility. Sci. Signal. 8, ra47.
Miyoshi, H., Adachi, T., 2014. Topography design concept of a tissue engineering scaffold for controlling cell function and fate through actin cytoskeletal modulation. Tissue Eng. Part B Rev. 20, 609–627.
Okeyo, K.O., Kurosawa, O., Oana, H., Kotera, H., Washizu, M., 2016. Minimization of cell-substrate interaction using suspended microstructured meshes initiates cell sheet formation by self-assembly organization. Biomed. Phys. Eng. Express 2, 065019.
Okeyo, K.O., Kurosawa, O., Yamazaki, S., Oana, H., Kotera, H., Nakauchi, H., Washizu, M., 2015. Cell adhesion minimization by a novel mesh culture method mechanically directs trophoblast differentiation and self-assembly organization of human pluripotent stem cells. Tissue Eng. Part C Methods 21, 1105–1115.
Okeyo, K.O., Tanabe, M., Kurosawa, O., Oana, H., Washizu, M., 2018. Self-organization of human iPS cells into trophectoderm mimicking cysts induced by adhesion restriction using microstructured mesh scaffolds. Dev. Growth Differ. 1, 1–13.
Ollion, J., Cochennec, J., Loll, F., Escudé, C., Boudier, T., 2013. TANGO: a generic tool for high-throughput 3D image analysis for studying nuclear organization. Bioinformatics 29, 1840–1841.
Riedl, J., Crevenna, A.H., Kessenbrock, K., Yu, J.H., Neukirchen, D., Bista, M., Bradke, F., Jenne, D., Holak, T.A., Werb, Z., Sixt, M., Wedlich-Soldner, R., 2008. Lifeact: a versatile marker to visualize F-actin. Nat. Methods 5, 605–607.
Rosowski, K., Mertz, A.F., Norcross, S., Dufresne, E.R., Horsley, V., 2015. Edges of human embryonic stem cell colonies display distinct mechanical properties and differentiation potential. Sci. Rep. 5, 14218.
Sagy, N., Slovin, S., Allalouf, M., Pour, M., Savyon, G., Boxman, J., Nachman, I., 2019. Prediction and control of symmetry breaking in embryoid bodies by environment and signal integration. Development 146, dev181917.
Shao, Y., Taniguchi, K., Gurdziel, K., Townshend, R.F., Xue, X., Yong, K.M.A., Sang, J., Spence, J.R., Gumucio, D.L., Fu, J., 2017. Self-organized amniogenesis by human pluripotent stem cells in a biomimetic implantation-like niche. Nat. Mater. 16, 419–425.
Shahbazi, M.N., Siggia, E.D., Zernicka-Goetz, M., 2019. Self-organization of stem cells into embryos: A window on early mammalian development. Science 364, 948–951.
Smith, K.N., Singh, A.M., Dalton, S., 2010. Myc represses primitive endoderm differentiation in pluripotent stem cells. Cell Stem Cell 7, 343–354.
Takata, N., Sakakura, E., Eiraku, M., Kasukawa, T., Sasai, Y., 2017. Self-patterning of rostral-caudal neuroectoderm requires dual role of Fgf signaling for localized Wnt antagonism. Nat. Commun. 8, 1339.
Takebe, T., Wells, J.M., 2019. Organoids by design. Science 364, 956–959.
Toyooka, Y., Shimosato, D., Murakami, K., Takahashi, K., Niwa, H., 2008. Identification and characterization of subpopulations in undifferentiated ES cell culture. Development 135, 909–918.
Verstreken, C.M., Labouesse, C., Agley, C.C., Chalut, C.C., 2019. Embryonic stem cells become mechanoresponsive upon exit from ground state of pluripotency. Open Biol. 9, 180203.
Warmflash, A., Sorre, B., Etoc, F., Siggia, E.D., Brivanlou, A.H., 2014. A method to recapitulate early embryonic spatial patterning in human embryonic stem cells. Nat. Methods 11, 847–854.
Xie, A.W., Binder, B.Y.K., Khalil, A.S., Schmitt, S.K., Johnson, H.J., Zacharias, N.A., Murphy, W.L., 2017. Controlled self-assembly of stem cell aggregates instructs pluripotency and lineage bias. Sci. Rep. 7, 14070.
Yang, S.-H., Kalkan, T., Morrisroe, C., Smith, A., Sharrocks, A.D., 2012. A genome-wide RNAi screen reveals MAP kinase phosphatases as key ERK pathway regulators during embryonic stem cell differentiation. PLoS Genet. 8, e1003112.